

Semi-Supervised Semantic Segmentation Via Label Reuse for Human Decomposition Images

Sara Mousavi, Zhenning Yang, Kelly Cross, Dawnie Steadman, Audris Mockus
 The University of Tennessee Knoxville, USA
 {mousavi, zyang37, kcross12, dsteadma, audris}@vols.utk.edu

Abstract

*Semantic segmentation is a challenging computer vision task demanding a significant amount of pixel-level annotated data. Producing such data is a time-consuming and costly process, especially for domains with a scarcity of experts, such as medicine or forensic anthropology. While numerous semi-supervised approaches have been developed to make the most from the limited labeled data and ample amount of unlabeled data, domain-specific real-world datasets often have characteristics that both reduce the effectiveness of off-the-shelf state-of-the-art methods and also provide opportunities to create new methods that exploit these characteristics. We propose and evaluate a semi-supervised method that reuses available labels for unlabeled images of a dataset by exploiting existing similarities, while dynamically weighting the impact of these reused labels in the training process. We evaluate our method on a large dataset of human decomposition images and find that our method, while conceptually simple, outperforms state-of-the-art consistency and pseudo-labeling-based methods for the segmentation of this dataset. **CAUTION: This paper includes graphic content of human decomposition.***

1. Introduction

Semantic segmentation has many applications in various domains. In particular, segmenting body parts in images of human decomposition is a critical first step needed to make large and unique photographic datasets of human decomposition usable in forensic research. First, the type and level of decomposition varies among body parts [14, 34] and separating body parts with segmentation allows studying the presence of forensic features on specific body parts (e.g. presence of mold on legs vs. hands). Second, it enables placing forensic features in context to pave the way for downstream models of time-of-death estimation that include forensic features and body parts as key predictors [3, 4, 16]. Finally, it enables separating body parts from

the background area and, therefore, helps with the identification of forensic features that can be very similar to the background (as shown in Figure 1).

Pixel-level annotations are necessary for accurate supervised semantic segmentation but may be too costly for many application domains. Manual pixel-level labeling needed for semantic segmentation can take 15 to 60 times longer than that of region-level and image-level labels [28]. In addition, specialized expertise is often necessary and scarce for labeling images in domains such as medicine or forensic anthropology. To address such challenges, many semi-supervised and weakly-supervised methods have been developed to work with relatively few labeled and numerous unlabeled or weakly labeled images.

Weakly-supervised segmentation methods [13, 26] rely on weakly annotated data to produce annotations for the unlabeled portion of the data. The newly produced annotations along with the original existing ones are then used in a supervised manner for the task of interest. However, due to the need for weak labels in such methods, recently, semi-supervised segmentation methods have gained more attention. Many semi-supervised segmentation methods have been developed mainly based on producing pseudo-labels for existing unlabeled images [2, 25, 35] or through consistency-based methods utilizing augmentations [24, 30, 38], perturbations [24], and multi-model collaborations [21].

While many of these methods have complex structures and their results highly depend on well-tailored perturbation techniques, in this work, we explore the possibility of exploiting intrinsic differences and similarities in the data itself. For example, in images depicting gradual growth or decay of subjects (plants or human bodies) from agriculture and anthropology domains, even though images depicting a specific instance of the same subject over time may look different, their annotation may be similar.

In this work, we tackle the problem of insufficient labels by presenting a semi-supervised method that exploits latent relationships among images. Our algorithm discovers such latent relationships in order to obtain pseudo-labels

for unlabeled images by first pairing the labeled images with similar unlabeled images and then reusing available pixel-level annotations for similar but unlabeled images in each pair. We define a multi-objective loss function that penalizes the predictions depending on the level of predicted annotation similarity between the images in each pair. In other words, the key idea is to exploit the similarity present in the image collection by re-using annotations for unlabeled images weighted by the extent of the network’s understanding of their label similarity while also jointly learning from supervised samples. We call our method SLRNet for Similarity-based Label Reuse Network. The code is available at: [redacted for review].

The human decomposition photographic collection used in this work is intended to support forensic research and casework, and contains over 1M photos taken from 500 decaying subjects over dynamic intervals often days or weeks apart. At each timestep, one or more images depicting each class (body part) are present.

Semantic segmentation of decaying body parts is complicated due to various reasons. First, the color and texture of decaying body parts and many forensic features such as mummified skin being extremely similar to the background (Figure 1). Second, in human decomposition imagery, subjects gradually evolve over time from the “fresh” stage to the completely decayed stage of “skeletonization”. Third, different body parts are difficult to distinguish due to environmental settings such as muddy ground, especially in late stages of decay. Finally, the often multi-day delay between photos, the lack of control in the camera view, changing weather conditions, disturbances caused by scavenging, and the lack of explicit links over time of classes limits the applicability of powerful video object segmentation (VOS) methods. However, the gradual decay of these subjects brings about a similarity attribute in such datasets that can be utilized towards developing an efficient but simple semi-supervised method.

In this work, we propose a simple method that reuses labeled data as pseudo-labels for unlabeled images. Specifically, we first use an unsupervised algorithm to identify immediately or transitively similar images to each labeled image. This algorithm exploits the fact that the images depicting the same evolving subjects are more similar if they



Figure 1. Examples of the background having a similar color and texture to the foreground in the human decomposition dataset.

are closer to each other on the decay spectrum, and the same subject may have a different appearance in early and late evolution stages, however have very similar annotations. We find similar images to a given labeled image among its neighbors recursively until no image with sufficiently high similarity is found. Pairs are then created between the annotated image and the similar images, with the annotation of the labeled images being applied to the unlabeled images as pseudo-labels. However, when training the segmentation network, we do not treat the losses from pseudo labels equally, but adjust them based on the level of similarity between the network’s predictions for the images in the pairs.

We evaluate our method on the human decomposition images and compare our method with two state-of-the-art semi-supervised semantic segmentation methods: CCT [31] and PseudoSeg [45]. Results indicate that SLRNet, while having a much simpler conceptual structure and correspondingly shorter run-time, outperforms both CCT and PseudoSeg on evolving images of human decomposition.

In the rest of this paper, we start from related work in Section 2 and the proposed method in Section 3. The dataset used in this work is presented in Section 3.1 and the pairing algorithm in Section 3.2. The training process is described in Section 3.3 and our results and conclusion are presented in Sections 4 and 5.

2. Related Work

2.1. Semi-Supervised Learning

Computer vision techniques are increasingly used to solve real-world problems in numerous domains, but the scarcity of clean labeled data hinders this progress. On one hand, supervised techniques need large training samples while unsupervised methods often do not achieve the desired accuracy. Semi-supervised methods [15, 20, 23, 27, 41] have emerged as a potential solution to this problem. They rely on a large set of unlabeled data and a limited labeled set and have recently achieved good performance. New efforts in this area take various approaches, such as the creation of pseudo-labels [2, 25, 35] or utilizing consistency-based techniques [23, 30, 38] to counter over-fitting, increase the training sample, find the optimal boundary between classes, and improve generality of the models.

Semi-supervised methods are either transductive [19, 29], where the goal is to generate labels for a set of unlabeled images, or inductive [24, 30, 38, 43], where the goal is to find a classifier that can predict labels for any image in the input space [40].

Transductive methods such as [19, 29] are based on label propagation to generate more training data. For example, Iscen et al. [19] use a transductive algorithm to generate pseudo-labels for unlabeled data. Liu et al. make use of labels from related domains and propagates them to generate

pseudo-labels for a target dataset [29]. Our work’s pairing algorithm is also inspired by transductive methods in order to obtain pseudo-labels for unlabeled images (Section 3.2).

Some inductive-based methods use unlabeled data along with labeled data in a supervised fashion by first generating pseudo-labels for unlabeled images and then using a combination of both labeled and pseudo-labeled images to learn from [43]. Other methods enforce a type of consistency across predictions for unlabeled data [24, 30, 38]. Consistency-based methods rely on the idea that a network’s predictions should be mostly similar across perturbations or slightly modified versions of the same input. For example, in the work by Laine et al. [24], consistency over augmented and dropped out versions of the input images is enforced. Similar to consistency-based methods we consider images in a pair as perturbed versions of each other, however, unlike those methods we do not enforce consistency on the predictions of the network. Instead we use these predictions to control the impact of the pseudo-labeled images on the network’s learning.

2.2. Semi-Supervised Semantic Segmentation

In addition to image classification tasks, semi-supervised methods are also used for semantic segmentation. Various methods [18, 31, 36, 44, 45] have been developed that achieve state-of-the-art on benchmark datasets such as VOC12 [12] and COCO [28] as well as domain specific data such as medical images [9, 33].

Consistency-based training has also been used for semantic segmentation with promising results. For example, CCT [31] is based on cross consistency learning and uses a segmentation network with an encoder and a decoder for annotated images. Additionally, CCT adds several auxiliary decoders that use perturbed versions of the encoder’s output for the unlabeled data. It then enforces consistency over the outputs of the auxiliary decoders and that of the main decoder. CCT has achieved state-of-the-art results on the VOC12 [12] dataset.

Other methods, such as PseudoSeg, combine ideas of pseudo-labeling and consistency learning [45]. The authors use a similar idea to consistency-based methods to generate pseudo-labels. They fuse a self attention-based GradCAM of an unlabeled input image to their network’s prediction for a weakly augmented version of that same input and use the result as a pseudo-label. Then, they enforce consistency between the predictions of the network for a strongly augmented version of that input and the pseudo-label.

The performance of methods such as CCT and PseudoSeg highly depends on the types of perturbations and augmentations used in the process. In this work, we present a simple method that does not rely on external augmentation and perturbation, and is conceptually simpler. The key idea of our method is to find a way to effectively reuse the exist-

ing differences and similarities in the dataset itself.

3. Method

Figure 2 shows an overview of our method, which consists of two main steps: image-pairing and network training. In the pairing step, we use an unsupervised method to identify unlabeled images that are similar to the labeled images, and therefore, can be paired with them. In the training phase, first, we simply reuse the annotation of the labeled images by assigning them as pseudo-labels to their similar but unlabeled match. We then use the image pairs along with the original labeled images as a separate set to train our semi-supervised semantic segmentation network in an end-to-end fashion. Our network is fed with both labeled images and the pairs at each iteration to jointly learn from both images with original labels and pseudo labels. Throughout the training, however, we use a custom loss function to control the effect of the unlabeled images and their pseudo-labels on the learning process with respect to the similarity of the two predictions for the images in the pairs as well as the current learning iteration.

In the following sections, we provide details on the dataset used in this work (Section 3.1), the unsupervised image pairing process (Section 3.2), and the network structure and its training process (Section 3.3).

3.1. Human Decomposition Dataset

The human decomposition dataset used in this work consists of photos taken from different body parts of various subjects donated to the forensic anthropology center of our university. The subjects were placed in an uncontrolled outdoor environment to record and track the decay process. The dataset has been collected over the years, with each subject staying in the facility for approximately one year. The photos are taken at various non-uniform intervals (one or more days apart) following a specific protocol. Each day, multiple images depicting various body parts for each subject are taken. The metadata associated with each image provides information about which donor the photo belongs to and the date at which the photo is taken. We denote these images by $\mathcal{I}_{d,n}$, where $d \in \{1, 2, \dots, D\}$, $n \in \{1, 2, \dots, N\}$. D is the total number of days photographed for each subject, N is the total number of images taken at any given day, and \mathcal{I} represents the set of all images for that subject. There exist 6 main categories namely “hand”, “arm”, “foot”, “leg”, “torso”, and “head”. In this work, we consider each body part as one class.

3.2. Unsupervised Image Pairing

The main idea of pairing labeled images with unlabeled ones is to utilize the potential reuse of annotation. It is likely for a dataset to have two or more images depicting the same content with only small differences. This is even more the

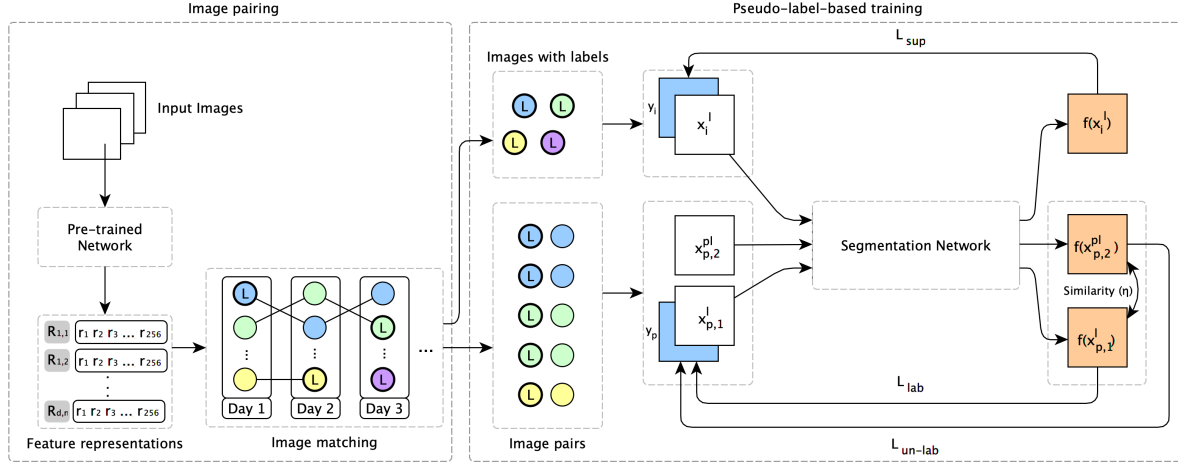


Figure 2. An overview of our method is shown (best seen in color). Images, first, go through a classification network which is pre-trained on ImageNet [10] and fine-tuned on the human decomposition data to be mapped to feature vectors. Labeled images (shown with circles labeled with ‘L’) and unlabeled images (circles with no labels) along with their feature vectors are then fed to our unsupervised image matching component to obtain similar images that can be paired with labeled ones and reuse the labels as pseudo-labels for the unlabeled images in the pairs. These pairs (one labeled image and one unlabeled image) along with the labeled images as a separate set, then go through our segmentation network that uses a customized loss function to control the effect of the pseudo-labels in the training process based on the similarity between the network’s predictions (η) for the pair.



Figure 3. A few pair examples generated using our pairing algorithm. The third pair from the first row is anonymized

case for image datasets with evolving content such as images of human decomposition, aging faces, growing plants, or decaying produce.

In the human decomposition dataset, while photos from the same subjects at early evolution stages can drastically differ from those at late stages in terms of visual features, they still tend to have similar annotations. For example, while a hand in the “fresh” stage might look different from a hand in the late stages of decay, their annotations still resemble a hand from the same body and have similarities. Moreover, images belonging to neighboring days are more likely to be similar as well. We leverage this characteristic and use neighbor-based comparison to identify the most suitable pairs for a given set of labeled images.

First, we use the feature maps of a pre-trained classification network such as ResNet to map all images to their corresponding feature representations. To do so, we feed the images into the classification network, excluding its last fully-connected and softmax layers, and use the output vectors as the feature representations. In this work, we used

ResNet50 [17] pre-trained on ImageNet [10] and fine-tuned with human decomposition data. This fine-tuning uses only image-level labels and increases the probability that similar images would contain the same body part. With ResNet, the vector length is 2048. Inspired by DeepCluster [5], we also reduce the length of these representations to 256 using Principle Component Analysis [42] to improve the overall run-time of our method. Through experiments we found that on average, using PCA, pairing takes 54.42% less time than without PCA. We denote the resulting feature representation for $I_{d,n}$ which is the n^{th} image in day d , as $R_{d,n}$.

To identify potential images to pair with the labeled image $I_{d,n}^l$ (marked with an l superscript), we compare its feature representation (i.e. $R_{d,n}^l$) with all other feature representations of its neighboring days and pick the most similar image as a match. From there, we recursively compare the matched images with their own respective neighbors to find other suitable pairs for the original $I_{d,n}^l$.

While this process can track similar images throughout different stages of decay, it also forces a match between each two neighboring days even if the difference is large. To circumvent this issue, we stop the matching process if the similarity of the two images being compared is lower than the overall average similarity calculated up to that point among the potential matches for $I_{d,n}^l$. Comparison of the image features is done through cosine similarity as: $Similarity(R_{d,n}, R_{d',m}) = \frac{R_{d,n} \cdot R_{d',m}}{\|R_{d,n}\| \cdot \|R_{d',m}\|}$. The pairing process is detailed in Alg. 1 where, for each labeled image, initially the “Compare” function is called for it and

Algorithm 1: Image matching algorithm

Result: Pairs of labeled and unlabeled images

```
Def Main():
    matches = {};
    for each labeled image  $I_{d,n}^l$  do
        Compare( $I_{d,n}^l, I_{d,n}^l$ );
    end
    pairs = [];
    for each labeled image  $I_{d,n}^l$  in matches do
        for each unlabeled match  $I_{d,n}^{ul}$  in matches[ $I_{d,n}^l$ ] do
            pairs.append( $I_{d,n}^l, I_{d,n}^{ul}$ );
        end
    end
end

Def Compare( $I, ref$ ):
    R = PCA(Feature( $ref$ ));
    for each neighboring day  $D$  for image  $ref$  do
        maxSim = 0;
        match = NULL;
        for each image  $I'$  in  $D$  do
            R' = PCA(Feature( $I'$ ));
            s = Similarity(R, R');
            if  $s > maxSim$  then
                maxSim = s;
                match =  $I'$ ;
            end
        end
        if  $maxSim \geq AvgSim(matches[I])$  then
            matches[I].add((match, maxSim));
            Compare( $I, match$ );
        end
    end
end
```

itself as “*ref*”. In the “*Compare*” function, each reference image (“*ref*”) is compared to all of its neighboring images and those that are found to be appropriate matches will be added to the list of images that can be paired with the labeled image ($I_{d,n}^l$). The “*Compare*” function is then recursively called for each image in the match set.

From the matches obtained for $I_{d,n}^l$, a few may coincidentally have labels. Those are removed from the group of images being paired with $I_{d,n}^l$ as they will be later paired with unlabeled matches of their own. A few example pairs are shown in Figure 3.

3.3. Network Structure and Training

we denote the set of labeled images by $\mathcal{I}^l = \{(x_1^l, y_1), (x_2^l, y_2), \dots, (x_L^l, y_L)\}$, where L is the total number of labeled images, y_i is the annotation for the i^{th} labeled image (i.e. x_i^l) and has dimensions of $W \times H \times C$ representing width, height and the number of classes, respectively.

We reuse the annotations of the labeled images by assigning them as pseudo-labels (marked with a pl superscript to denote that they have pseudo-labels) to the image with no labels in the pairs obtained from our image pairing algorithm described in the previous section (3.2). We denote the pairs with: $\mathcal{P} =$

$$\left\{ \left((x_{1,1}^l, x_{1,2}^{pl}), y_1 \right), \left((x_{2,1}^l, x_{2,2}^{pl}), y_2 \right), \dots, \left((x_{P,1}^l, x_{P,2}^{pl}), y_P \right) \right\}.$$

where P is the total number of pairs and $x_{p,1}^l$ and $x_{p,2}^{pl}$ are the first labeled and second pseudo-labeled elements in the p th pair respectively. In this setting $\{x_{1,1}^l, x_{2,1}^l, \dots, x_{P,1}^l\} \subset \mathcal{I}^l$ and these are not unique images, whereas $\{x_{1,2}^{pl}, x_{2,2}^{pl}, \dots, x_{P,2}^{pl}\}$ are P unique unlabeled images. That is because a labeled image could be paired with more than one image.

It is important to note that there may not exist an unlabeled match for every single image in the labeled set. Therefore, we feed the labeled images in a separate set, parallel to the pairs, even though some of them might be already included in the pair branch, to ensure the inclusion of all labeled images in the training process.

Additionally, as is expected, the location and orientation of the body parts captured in an unlabeled image may not be perfectly aligned with that of the labeled image in the pair even though the photos are taken following a specific protocol. Therefore, we introduce a custom loss function to control the impact of the pseudo-labels on the learning process with respect to the level of similarity between the network’s predicted labels for the two images in the pair.

Our objective is to exploit the additional pseudo-labeled images to improve the performance of the semantic segmentation network. In this method, we use a semantic segmentation network with a multi-objective loss function to facilitate learning from both labeled and pseudo-labeled images. At each iteration, the network is fed with a labeled image and a pair of images. We calculate a supervised loss and a loss for pairs, following Eq. 1 and Eq. 2 respectively. In the supervised loss calculated for the labeled images (Eq. 1), CE is cross entropy calculated using the ground truth y_i and the predicted labels for input x_i^l which is shown by $y'_i = f(x_i^l)$.

$$\mathcal{L}_{sup} = \frac{1}{|\mathcal{I}^l|} \sum_{x_i^l, y_i \in \mathcal{I}^l} CE(y_i, y'_i) \quad (1)$$

Next, we calculate a loss for the pairs. As mentioned above, each pair has one labeled and one unlabeled image. We calculate pair loss following Eq. 2.

$$\begin{aligned} \mathcal{L}_{pair} = \mathcal{L}_{lab} + \mathcal{L}_{un-lab} &= \frac{1}{|\mathcal{P}|} \sum_{x_{1,i}^l, y_i \in \mathcal{P}} CE(y_i, f(x_{1,i}^l)) \\ &+ \frac{1}{|\mathcal{P}|} \sum_{x_{2,i}^{pl}, y_i \in \mathcal{P}} \lambda * \eta * CE(y_i, f(x_{2,i}^{pl})) \end{aligned} \quad (2)$$

where $i \in \{1, 2, \dots, P\}$. The first and the second part of the loss are calculated based on the labeled image, y_i and $f(x_{1,i}^l)$, and the unlabeled image, y_i and $f(x_{2,i}^{pl})$, in the pair respectively. Since y_i are not actual labels for $x_{2,i}^{pl}$, the loss

calculated based on them is weighted by a similarity-based weight, η , and an iteration-based weight, λ . We use the prediction of the network for the pair, to determine the level of contribution for the loss calculated based on the pseudo labels in the backpropagation and calculate η accordingly. The idea is to use the network’s understanding to measure how similar and aligned the annotations for the images in a pair are. We compare the prediction of the network for the images in the pair to each other. The higher the similarity, the larger the weight will be. If the prediction of the network for the two images is different, the images may not be well aligned and the weight for the loss calculated based on the pseudo-label will be smaller. η is at most 1.

$$\eta = \frac{f(x_{1,i}^l) \cap f(x_{2,i}^{pl})}{(W \times H)_{x_{1,i}^l}} \quad (3)$$

where W and H are the width and the height for $x_{1,i}^l$ respectively. Furthermore, $f(x_{1,i}^l)$ and $f(x_{2,i}^{pl})$ are the predictions of the network for $x_{1,i}^l$ and $x_{2,i}^{pl}$ respectively.

Additionally, since the network’s prediction is not robust at early epochs, we use λ calculated based on the iteration numbers to minimize the influence of the initial noisy predictions and incorrect use of the pseudo labels in the training process. The value of λ linearly increases with training iteration and is at most 1.

$$\lambda = \frac{(\text{epoch} * \text{ipe} + \text{iter})}{\text{max_iters}} \quad (4)$$

where epoch is the current epoch, ipe is the number of iterations per each epoch, iter is the current iteration, and max_iter is the total number of epochs \times ipe . The network is trained to minimize the overall loss:

$$\mathcal{L} = \mathcal{L}_{sup} + \mathcal{L}_{pair} \quad (5)$$

4. Experimental Results

In this section, we provide implementation details and an evaluation of our method.

4.1. Implementation Details

We implemented our method using HRNetV2 [37], Xception [7] and ResNet [17] as the backbones built on the MIT implementation [39]. We implemented SLRNet using the PyTorch framework [32]. We trained our method on a single *TeslaV100 – SXM2* GPU with *32GB* memory. To train the segmentation network, we used Stochastic Gradient Descent (SGD) [22] with momentum of 0.9 and weight decay of 10^{-4} . We started with a learning rate of 0.02. The learning rate is gradually decreased using polynomial decay with power 0.9 [6]. We used the number of train samples divided by batch size as iterations per epoch.

4.2. Dataset and Evaluation Metric

The human decomposition dataset includes 1864 annotated images for “hand”, “arm”, “foot”, “leg”, “torso”, and “head” classes. We use 60%, 20%, 20% ratio to create training, validation and test sets. As a result, we have 1118, 373, and 373 images in our training, validation and test sets respectively. Additionally, we use 5906 unlabeled images resulted from identifying matches for the labeled images in the training set with other unlabeled images in the dataset using our pairing algorithm. Similar to other semantic segmentation works [18, 31, 36], we use the mean intersection-over-union (mean IoU) and pixel accuracy as evaluation metrics. We also provide additional evaluation for a plant dataset (that shares similar characteristics to the human decomposition dataset) in the supplementary material.

4.3. Comparisons to Previous Work

To the best of our knowledge, we are the first to explore semantic segmentation for images with evolving content such as human decomposition data and therefore there are no similar benchmarks or state-of-the-art methods on this topic. Therefore, to evaluate the effectiveness of our method, we quantitatively compare it with previous general state-of-the-art semi-supervised semantic segmentation methods, namely CCT [31] and PseudoSeg [45].

CCT is a consistency-based method that enforces consistency to the network’s predictions for various perturbed version of an input. It uses a two branch training structure one for labeled and one for unlabeled data. The two branches share the same encoder and one decoder. On the unsupervised branch it uses $K = 7$ auxiliary decoders and various perturbations and enforces consistency between their outputs and the output from the main shared decoder on the same input through a loss function.

PseudoSeg uses a mix of pseudo-labeling and consistency-based training to leverage unlabeled images in the network’s learning [45]. In PseudoSeg, the pseudo-labels are generated by fusing the network prediction for a weakly augmented input image and the self-attention GradCAM generated for that input. In the training process, the authors use a similar idea to consistency-based methods and force their network’s prediction for a strongly augmented version of the same input to be consistent with the pseudo-label that resulted from the fusion process.

To compare our method to CCT and PseudoSeg, we applied their semi-supervised setting to our data and compared the results with those obtained using our method. CCT and PseudoSeg use both labeled and unlabeled images to learn from them jointly. We use the unlabeled images obtained from our pairing algorithm and the labeled images as their unlabeled and labeled training inputs, respectively. We use the same validation and test sets for our method, CCT, and

Table 1. Mean-IoU, mean-pixel accuracy, per class IoU, and run-time for CCT, PseudoSeg and SLRNet on the test data. The results indicate that our method consistently outperforms other methods on most classes with a large margin. Results are in percentages.

	Backbone	mIoU	mAcc	Per Class IoU							Run time
				BG	Foot	Hand	Arm	Leg	Torso	Head	
CCT	ResNet	62.77	86.67	88.73	52.16	53.29	48.56	63.39	60.67	72.57	23967m26s
PseudoSeg	Xception	62.22	86.62	88.45	48.47	49.11	43.88	61.51	63.93	80.16	1334m5s
	ResNet	62.49	86.99	88.56	45.84	47.16	50.46	62.74	64.04	78.59	1500m17s
Our Method	Xception	66.76	88.27	88.63	78.63	78.63	78.63	78.63	78.63	78.63	1300m19s
	ResNet	65.3	87.12	87.44	57.28	58.07	49.68	64.32	64.75	75.59	764m15s
	HRNet	72.42	90.04	90.01	62.42	67.9	61.06	69.5	72.06	83.98	708m24s

Table 2. Ablation study to examine the effect of λ , η , the additional unlabeled data produced using our pairing algorithm, and the quality of the pairs on the overall performance of our method with different backbones. Results are in percentages.

	Labeled Images	Pairs	λ	η	HRNet		ResNet		Xception	
					mIoU	mAcc	mIoU	mAcc	mIoU	mAcc
Supervised	✓	✗	✗	✗	68.42	88.86	47.38	80.11	61.15	86.39
	✓	✓	✗	✗	61.37	85.94	54.53	82.04	63.46	86.44
Semi-supervised	✓	✓	✗	✓	63.97	86.24	60.71	85.05	63.65	88.71
	✓	✓	✓	✗	67.18	88.37	59.89	84.53	62.24	86.41
	✓	✓	✓	✓	72.42	90.04	65.3	87.12	66.76	88.27
Semi-supervised	✓	Random	✓	✓	69.43	89.38	58.53	85.81	62.85	86.84

PseudoSeg. The results of comparing our method to CCT and PseudoSeg are shown Table 1.

The results indicate that our method outperforms both CCT and PseudoSeg using the mean-IoU and mean-Acc metrics with a few minor exceptions for “BG”, “Arm”, and “Head” classes in PseudoSeg. The results also confirm that, in general, the HRNet backbone captures spatial information better and performs well even for classes that occupy fewer pixels than the others and outperforms the other backbones for all methods. In the human decomposition data used in this work, this difference is pronounced due to the need to maintain multiple feature resolutions since we have images of the same class with varying views. Furthermore, the run-time reported in Table 1 shows that SLRNet has a shorter run time than CCT and PseudoSeg while having a conceptually simpler structure.

4.4. Image Pairing Evaluation

To evaluate the pairing component of SLRNet, we first analyzed the effect of the quality of the pairs on the performance by replacing them with random ones where each labeled image is paired with a random unlabeled image. The results in Table 2 show that using random pairs reduces the performance of the model as expected.

We further evaluated the pairing algorithm by examining to what degree the generated pairs represent the same

classes. To do so, we selected the top 5 subjects with the highest number of labeled images, for which 107 images were pixel-level labeled. Applying our pairing algorithm to this data resulted in 1343 pairs. To perform this evaluation, we manually image-level labeled unlabeled images in the pairs. This experiment showed that in 95.06% of the pairs, both images represented the same classes. We also evaluated our pairing algorithm’s quality by comparing the IoU of the labels in pairs generated using our algorithm with the mean and median IoUs of all possible pairs from same-class images in our labeled data, chosen as a baseline. Our pairs resulted in mean and median IoUs of 47.36% and 41.15% while pairing all same-class images resulted in 24.7% and 19.18% mean and median IoUs, respectively, indicating that our method was able to select higher quality matches than the average quality of matches in same-class pairs.

4.5. Ablation Study

SLRNet, as a whole, uses both labeled and paired images, weights the loss calculated based on the pseudo-labels using η , and reduces the initial noisy and unstable behavior of the network using λ . We conduct an ablation study by assessing the performance of our method in the absence of these components. The scenarios shown in Table 2 are 1) the presence of labeled images, pairs, λ , and η , 2) the presence of labeled images, pairs, and η and the absence of λ ,

3) the presence of labeled images, pairs, and λ and the absence of η , 4) the presence of labeled images, pairs and the absence of both λ and η , 5) the presence of labeled images and the absence of pairs, λ , and η . When η is absent, it means there is no similarity-based weighting for the loss calculated based on pseudo-labels. That means the pseudo-labels are used as actual ground-truths and the network is basically trained in a supervised fashion on both labeled images and those in pairs. The scenario with labeled images and no pairs, no λ , and no η is equivalent to a fully supervised version of our method when it is only trained on the 1118 labeled images.

The results of the ablation study indicate that our method performs its best when we include the additional unlabeled data produced using our pairing algorithm as well as using both λ and η to avoid initial noisy prediction of the network and control the contribution of the pseudo-labels in the training process. In addition, we observe that the supervised version of HRNetV2 performs better than the semi-supervised version of other backbones, and the additional data from pairs without being carefully controlled by η and λ would hurt its performance. That is because HRNet maintains multiple high-resolution features in parallel throughout its training and exchanges information between them via a multi-scale fusion. HRNetV2 specifically outputs four-resolution representations containing rich and precise spatial information; therefore, it outperforms other backbones in supervised training, but it can be potentially more sensitive to noise if it is not controlled by η and λ .

Furthermore, we qualitatively evaluate the performance of our method by providing the resulted segmentation for a few examples from using CCT, PseudoSeg, and SLRNet (examples shown in Figure 4). Results indicate that our method captures classes and their annotations more accurately and is more conservative with less false positives and more false negatives (first and third row) compared to CCT and PseudoSeg. We believe the reason is because of how our “reuse” technique promotes regions that are shared between pairs amalgamating to more conservative masks.

4.6. Limitations

The key assumption of SLRNet is that the image collection contains unannotated images that are sufficiently similar to annotated images. Furthermore, these similar images contain annotations that are similarly located. Such instances tend to be common in collections where the same or similar object or subject occurs in multiple images as in our case of human decomposition and growing plants. Our approach may not be suitable for image collections that do not exhibit this property as illustrated in supplemental materials for VOC12 dataset. In this dataset a subject or an object is almost never photographed multiple times, so its annotation can not be re-used. Also, such datasets do not

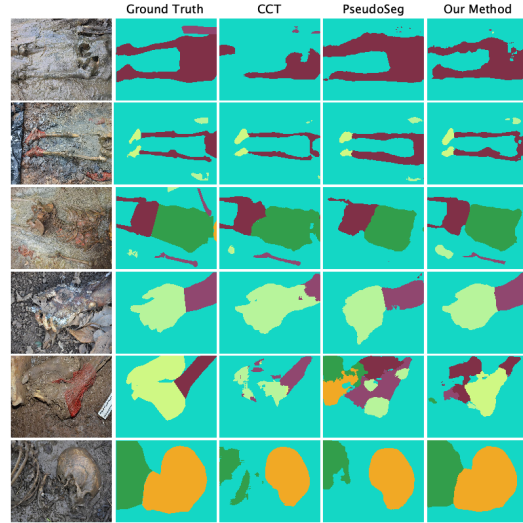


Figure 4. Examples of SLRNet and those from CCT and PseudoSeg on the human decomposition dataset when all methods are trained on 1118 labeled images and 5906 unlabeled images.

follow a specific photography protocol (common in many industry and research datasets) that may help partially align the annotations. In research and industry practice, the image collections very often contain repeated and similar images that are taken using a specific protocol. We, therefore, believe that the assumptions needed for SLRNet to perform on real datasets well are satisfied quite often. In these cases, SLRNet first identifies such opportunities where images are similar to one another and second adjusts for their potential annotation misalignments.

5. Conclusion

In this paper, we presented SLRNet, a simple semi-supervised technique for semantic segmentation of human decomposition data. The data at hand is a large image collection of decaying body parts with significant importance to the forensic community. Characteristically, the images in the data evolve through time as body parts decay and few labels are available due to the cost and scarcity of domain experts. Our main idea is to exploit image similarities and transfer labels from labeled to similar unlabeled images. To handle instances where the otherwise similar images do not contain the target in the same location, we structured a loss function to controls their level of impact on the network’s learning. We tested our method on a subset of our human decomposition imagery with 1118 labeled images and 5906 unlabeled images. Results show that our method outperforms the state-of-the-art CCT and PseudoSeg methods in semantic segmentation task of human decomposition data, while being faster and less conceptually complex.

6. Supplementary Material

In the main paper we have evaluated our method on an image dataset depicting decomposing human bodies. In this supplementary material, we first evaluate the generality of our proposed method for such datasets by conducting similar experiments on a dataset from a different domain capturing growing plants (Arabidopsis leaves from the Aberystwyth Leaf Evaluation Dataset [1]). Image data depicting different stages of growing plants manifest similarities to the human decomposition photos as both are depicting gradual changes over time that, over the full course of observation, lead to dramatic changes in appearance, but provide local similarities between neighboring timesteps that our method can leverage. Second, we provide more analysis on how a dataset such as the human decomposition data is different than a benchmark dataset such as VOC12. Finally, we provide some edge cases for the pairs generated using our pairing algorithm from the human decomposition data. **CAUTION: This paper includes graphic content of human decomposition.**

7. SLRNet for a Growing Plant Dataset

In this section we examine the applicability of SLRNet for a similar dataset to the human decomposition dataset; Aberystwyth Leaf Evaluation dataset.

7.1. Aberystwyth Leaf Evaluation Dataset

Aberystwyth Leaf Evaluation dataset is released by Aberystwyth University and has been collected to support researchers to further advance state-of-the-art methods used in image analysis for studying plants [1]. The images are collected by periodically taking pictures from Arabidopsis plants with 15-minute intervals using a robotic greenhouse system. The Aberystwyth dataset includes manual annotations for a subset of these image. The gradual growth of these plants results in a similar characteristic to the human decomposition data and provides an opportunity to utilize the limited available annotations and reuse them for the unlabeled images. An example showing a sequence of these images is shown in Figure 5.

The Aberystwyth Leaf dataset records the growth of Arabidopsis Thaliana plants potted in four trays. This dataset includes 134,040 Arabidopsis Thaliana plant images, from which 916 are manually annotated.

We use the same ratio as the human decomposition data, 60%, 20%, 20%, to create training, validation, and test sets respectively. Using our pairing algorithm, we use an additional 31,440 individual Arabidopsis plant images paired with the labeled ones in the training process. A few paired examples are shown in Figure 6. In our experiments with this dataset, we set the number of classes to two, for “background” and “leaf”.

Table 3. Supervised vs. semi-supervised comparisons of SLRNet with different backbones for segmenting images of Aberystwyth Leaf dataset. Results are shown in percentages.

	SLRNet			
	Supervised		Semi-supervised	
	mIoU	mAcc	mIoU	mAcc
HRNet	92.43	97.28	94.27	98.03
ResNet	88.17	95.64	94.2	98.01
Xception	63.53	83.94	65.13	86.99

7.2. Experimental Results for Aberystwyth Leaf Evaluation Dataset

We conducted two sets of experiments. First, to see the impact of the additional unlabeled data on the performance of our method in segmenting the Aberystwyth Leaf images, we compared the supervised version, when the model is only trained on the labeled data, vs. a semi-supervised version, when the model is trained on both labeled images and the pairs generated using our pairing algorithm. Second, we compared the performance of our method to that of two state-of-the-art methods, CCT [31] and PseudoSeg [45] using the ResNet backbone for a fair comparison to CCT.

The result of the two experiments are shown in Tables 3 and 4. The results in Table 3 indicate that our method (SLRNet) indeed facilitates controlled use of the additional unlabeled data and the semi-supervised setting that includes this data performs noticeably better as compared to the supervised version. Furthermore, Table 4 shows the results of comparing SLRNet with CCT and PseudoSeg. The results indicate that our method consistently outperforms both CCT and PseudoSeg methods in all metrics. Notably, PseudoSeg and SLRNet perform much better on the plant dataset. This is not particularly surprising since only two classes are predicted (leaf and background) for plants in contrast to a much harder problem of 7 classes for human decomposition. Additionally, CCT performed considerably worse than the other two methods in terms of its mean IoU. We suspect that CCT’s complex structure and its various perturbations hinder its prediction of small leaves. Figure 7 shows the predictions of these three methods for a few examples from Aberystwyth Leaf dataset. In summary, we found SLRNet to perform well on two unrelated photographic datasets, suggesting that it may be more generally applicable for datasets depicting subjects with gradual evolution.

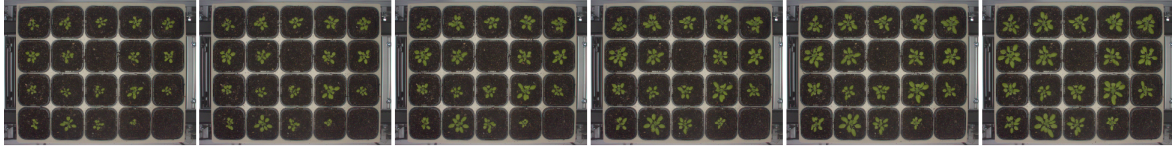


Figure 5. A set of example illustrating the gradual changes due to the growth.

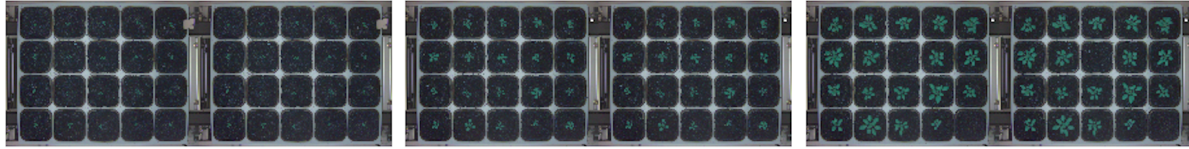


Figure 6. A few examples of pairing. Each labeled image is paired with an unlabeled image using our pairing algorithm.

8. Comparing Human Decomposition Images to Benchmark Datasets

SLRNet targets datasets representing evolving phenomena that have high potential for annotation reuse such as images of human decomposition, aging faces, growing plants, or decaying produce. Knowing the structure of such datasets and their gradual changes, such datasets are more likely to include images that can potentially have similar annotations (pixel-level labels). To confirm this hypothesis, we experimented on the Cityscape [8], VOC [11], and the human decomposition datasets. For each dataset, we first generated pairs of images depicting the exact same classes. We then calculated the intersection over union (IoU) between the labels of images in each pair to see how similar and align the labels of these images are. Normalized histograms of these calculated IoUs in Figure 8 show the result for this experiment. The result indicates that even though we have pairs of images with the same classes in all datasets, in the human decomposition dataset, these pairs tend to have similar masks with higher IoU than benchmark datasets VOC12 and Cityscape.

9. Edge Cases of the Human Decomposition Pairs

Based on the result provided in Section 4.4 in the main paper, our pairing algorithm is capable of pairing images from the same classes together (95.06% of the time). In this section we provide a few edge cases that can happen due to background-foreground similarity of the images. For example in Figure 9a, a decayed hand and foot are paired together. In addition, Figure 9b shows a pair in which images are not perfectly aligned but some part of the labels are still shared and reusable.

Manual observation of these pairs indicates that mismatch of classes rarely happens and that is when the back-

ground is a large portion of the image and the subjects in the two images are similar such as the example shown in Figure 9a. Additionally, due to the characteristic of this dataset, even not perfectly aligned pairs as shown in Figure 9b still provide correct a usable mask for some portion of the unlabeled images.

References

- [1] Jonathan Bell and Hannah M. Dee. Aberystwyth leaf evaluation dataset, Nov. 2016. [9](#)
- [2] David Berthelot, Nicholas Carlini, Ian Goodfellow, Nicolas Papernot, Avital Oliver, and Colin Raffel. Mixmatch: A holistic approach to semi-supervised learning. *arXiv preprint arXiv:1905.02249*, 2019. [1, 2](#)
- [3] Anna GC Boef, Olaf M Dekkers, Jan P Vandenbroucke, and Saskia le Cessie. Sample size importantly limits the usefulness of instrumental variable methods, depending on instrument strength and level of confounding. *Journal of clinical epidemiology*, 67(11):1258–1264, 2014. [1](#)
- [4] İsmail Cantürk and Lale Özyılmaz. A computational approach to estimate postmortem interval using opacity development of eye for human subjects. *Computers in biology and medicine*, 98:93–99, 2018. [1](#)
- [5] Mathilde Caron, Piotr Bojanowski, Armand Joulin, and Matthijs Douze. Deep clustering for unsupervised learning of visual features. In *Proceedings of the European Conference on Computer Vision (ECCV)*, pages 132–149, 2018. [4](#)
- [6] Liang-Chieh Chen, George Papandreou, Iasonas Kokkinos, Kevin Murphy, and Alan L Yuille. Deeplab: Semantic image segmentation with deep convolutional nets, atrous convolution, and fully connected crfs. *IEEE transactions on pattern analysis and machine intelligence*, 40(4):834–848, 2017. [6](#)
- [7] François Chollet. Xception: Deep learning with depthwise separable convolutions. In *Proceedings of the IEEE conference on computer vision and pattern recognition*, pages 1251–1258, 2017. [6](#)
- [8] Marius Cordts, Mohamed Omran, Sebastian Ramos, Timo Rehfeld, Markus Enzweiler, Rodrigo Benenson, Uwe

Table 4. Mean-IoU and mean-pixel accuracy for CCT, PseudoSeg and SLRNet on the Aberystwyth Leaf test data using the ResNet backbone.

	Mean-IoU (%)	Mean-Acc (%)	Per class IoU (%)	
			BG	Leaf
CCT	51.73	82.59	81.71	21.75
PseudoSeg	90.64	96.7	95.92	85.35
SLRNet	94.2	98.01	97.52	90.88

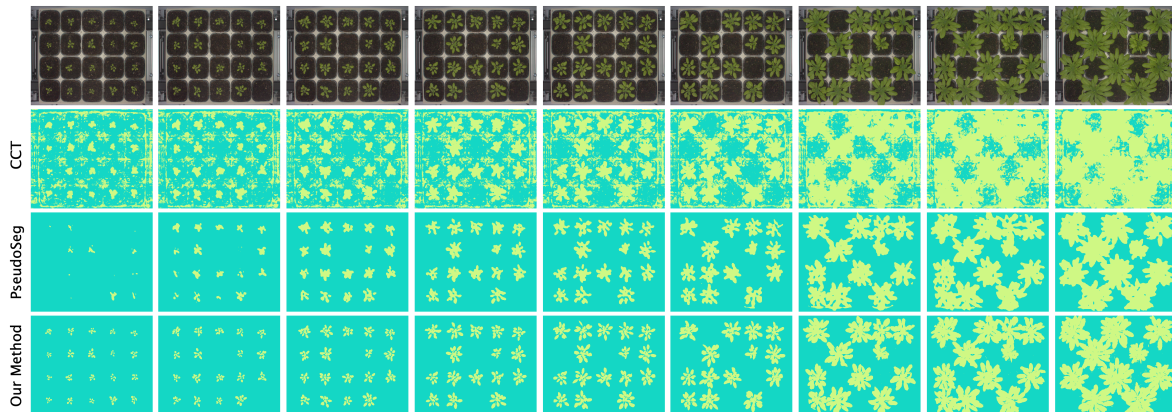


Figure 7. A few examples of performing semantic segmentation on the Aberystwyth Leaf dataset when using SLRNet, CCT and PseudoSeg.

- Franke, Stefan Roth, and Bernt Schiele. The cityscapes dataset for semantic urban scene understanding. In *The IEEE Conference on Computer Vision and Pattern Recognition (CVPR)*, June 2016. 10
- [9] Etienne Decencière, Xiwei Zhang, Guy Cazuguel, Bruno Lay, Béatrice Cochener, Caroline Trone, Philippe Gain, Richard Ordonez, Pascale Massin, Ali Erginay, et al. Feedback on a publicly distributed image database: the messidor database. *Image Analysis & Stereology*, 33(3):231–234, 2014. 3
- [10] Jia Deng, Wei Dong, Richard Socher, Li-Jia Li, Kai Li, and Li Fei-Fei. Imagenet: A large-scale hierarchical image database. In *2009 IEEE conference on computer vision and pattern recognition*, pages 248–255. Ieee, 2009. 4
- [11] Mark Everingham, Luc Van Gool, Christopher KI Williams, John Winn, and Andrew Zisserman. The pascal visual object classes challenge 2007 (voc2007) results. 2007. 10
- [12] Mark Everingham, Luc Van Gool, Christopher KI Williams, John Winn, and Andrew Zisserman. The pascal visual object classes (voc) challenge. *International journal of computer vision*, 88(2):303–338, 2010. 3
- [13] Hao-Shu Fang, Guansong Lu, Xiaolin Fang, Jianwen Xie, Yu-Wing Tai, and Cewu Lu. Weakly and semi supervised human body part parsing via pose-guided knowledge transfer. *arXiv preprint arXiv:1805.04310*, 2018. 1
- [14] Alison Galloway, Walter H Birkby, Allen M Jones, Thomas E Henry, and Bruce O Parks. Decay rates of human remains in an arid environment. *Journal of Forensic Science*, 34(3):607–616, 1989. 1
- [15] Yaroslav Ganin, Evgeniya Ustinova, Hana Ajakan, Pascal Germain, Hugo Larochelle, François Laviolette, Mario Marchand, and Victor Lempitsky. Domain-adversarial training of neural networks, 2016. 2
- [16] HT Gelderman, CA Kruiver, RJ Oostra, MP Zeegers, and WLJM Duijst. Estimation of the postmortem interval based on the human decomposition process. *Journal of Forensic and Legal Medicine*, 61:122–127, 2019. 1
- [17] Kaiming He, Xiangyu Zhang, Shaoqing Ren, and Jian Sun. Deep residual learning for image recognition. In *Proceedings of the IEEE conference on computer vision and pattern recognition*, pages 770–778, 2016. 4, 6
- [18] Wei-Chih Hung, Yi-Hsuan Tsai, Yan-Ting Liou, Yen-Yu Lin, and Ming-Hsuan Yang. Adversarial learning for semi-supervised semantic segmentation. *arXiv preprint arXiv:1802.07934*, 2018. 3, 6
- [19] Ahmet Iscen, Giorgos Tolias, Yannis Avrithis, and Ondrej Chum. Label propagation for deep semi-supervised learning. In *Proceedings of the IEEE conference on computer vision and pattern recognition*, pages 5070–5079, 2019. 2
- [20] Tarun Kalluri, Girish Varma, Manmohan Chandraker, and C V Jawahar. Universal semi-supervised semantic segmentation, 2019. 2
- [21] Zhanghan Ke, Kaican Li Di Qiu, Qiong Yan, and Rynson WH Lau. Guided collaborative training for pixel-wise

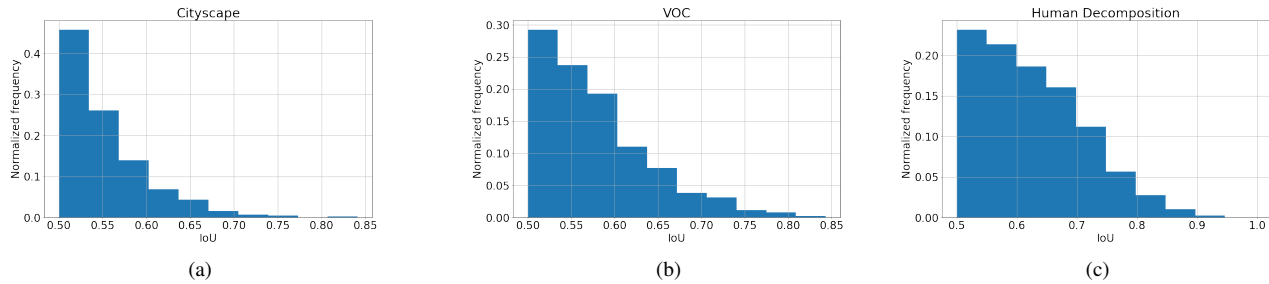


Figure 8. Histogram of IoU between pairs of labels for images with the same classes for Cityscape, Pascal VOC, and the human decomposition datasets are shown. The plots indicate that in a dataset with evolving content (gradual changes over time) such as the human decomposition dataset, there exist more label IoU similarity than others.



(a) Example of a pair with different classes



(b) Example of an unaligned pair

Figure 9. (a) shows examples of pairing images from different classes together. (b) shows examples of pairs with same classes but not perfectly aligned. Images are blurred due to their graphic nature.

semi-supervised learning. In *ECCV*, volume 2, page 6. Springer, 2020. 1

- [22] Nikhil Ketkar. Stochastic gradient descent. In *Deep learning with Python*, pages 113–132. Springer, 2017. 6
- [23] Samuli Laine and Timo Aila. Temporal ensembling for semi-supervised learning, 2017. 2
- [24] Samuli Matias Laine and Timo Oskari Aila. Temporal ensembling for semi-supervised learning, Apr. 12 2018. US Patent App. 15/721,433. 1, 2, 3
- [25] Dong-Hyun Lee et al. Pseudo-label: The simple and efficient semi-supervised learning method for deep neural networks. In *Workshop on challenges in representation learning, ICML*, volume 3, 2013. 1, 2
- [26] Jungbeom Lee, Eunji Kim, Sungmin Lee, Jangho Lee, and Sungroh Yoon. Ficklenet: Weakly and semi-supervised semantic image segmentation using stochastic inference. In *Proceedings of the IEEE conference on computer vision and pattern recognition*, pages 5267–5276, 2019. 1
- [27] Tsung-Yi Lin, Michael Maire, Serge Belongie, Lubomir Bourdev, Ross Girshick, James Hays, Pietro Perona, Deva Ramanan, C. Lawrence Zitnick, and Piotr Dollár. Microsoft coco: Common objects in context, 2015. 2
- [28] Tsung-Yi Lin, Michael Maire, Serge Belongie, James Hays, Pietro Perona, Deva Ramanan, Piotr Dollár, and C Lawrence Zitnick. Microsoft coco: Common objects in context. In *European conference on computer vision*, pages 740–755. Springer, 2014. 1, 3
- [29] Bin Liu, Zhirong Wu, Han Hu, and Stephen Lin. Deep metric transfer for label propagation with limited annotated data. In *Proceedings of the IEEE International Conference on Computer Vision Workshops*, pages 0–0, 2019. 2, 3
- [30] Takeru Miyato, Shin-ichi Maeda, Masanori Koyama, and Shin Ishii. Virtual adversarial training: a regularization method for supervised and semi-supervised learning. *IEEE transactions on pattern analysis and machine intelligence*, 41(8):1979–1993, 2018. 1, 2, 3
- [31] Yassine Ouali, Céline Hudelot, and Myriam Tami. Semi-supervised semantic segmentation with cross-consistency training. In *Proceedings of the IEEE/CVF Conference on Computer Vision and Pattern Recognition*, pages 12674–12684, 2020. 2, 3, 6, 9
- [32] Adam Paszke, Sam Gross, Francisco Massa, Adam Lerer, James Bradbury, Gregory Chanan, Trevor Killeen, Zeming Lin, Natalia Gimelshein, Luca Antiga, et al. Pytorch: An imperative style, high-performance deep learning library. *Advances in neural information processing systems*, 32, 2019. 6
- [33] Prasanna Porwal, Samiksha Pachade, Ravi Kamble, Manesh Kokare, Girish Deshmukh, Vivek Sahasrabudde, and Fabrice Meriaudeau. Indian diabetic retinopathy image dataset (idrid): a database for diabetic retinopathy screening research. *Data*, 3(3):25, 2018. 3
- [34] Tal Simmons, Rachel E Adlam, and Colin Moffatt. Debugging decomposition data—comparative taphonomic studies and the influence of insects and carcass size on decomposition rate. *Journal of forensic sciences*, 55(1):8–13, 2010. 1
- [35] Kihyuk Sohn, David Berthelot, Chun-Liang Li, Zizhao Zhang, Nicholas Carlini, Ekin D Cubuk, Alex Kurakin, Han Zhang, and Colin Raffel. Fixmatch: Simplifying semi-

- supervised learning with consistency and confidence. *arXiv preprint arXiv:2001.07685*, 2020. 1, 2
- [36] Nasim Souly, Concetto Spampinato, and Mubarak Shah. Semi supervised semantic segmentation using generative adversarial network. In *Proceedings of the IEEE international conference on computer vision*, pages 5688–5696, 2017. 3, 6
- [37] Ke Sun, Yang Zhao, Borui Jiang, Tianheng Cheng, Bin Xiao, Dong Liu, Yadong Mu, Xinggang Wang, Wenyu Liu, and Jingdong Wang. High-resolution representations for labeling pixels and regions. *arXiv preprint arXiv:1904.04514*, 2019. 6
- [38] Antti Tarvainen and Harri Valpola. Mean teachers are better role models: Weight-averaged consistency targets improve semi-supervised deep learning results. In *Advances in neural information processing systems*, pages 1195–1204, 2017. 1, 2, 3
- [39] MIT Computer Vision team. semantic-segmentation-pytorch. <https://github.com/CSAILVision/semantic-segmentation-pytorch>, 2021. 6
- [40] Jesper E Van Engelen and Holger H Hoos. A survey on semi-supervised learning. *Machine Learning*, 109(2):373–440, 2020. 2
- [41] Jason Weston, Frédéric Ratle, Hossein Mobahi, and Ronan Collobert. Deep learning via semi-supervised embedding. In *Neural networks: Tricks of the trade*, pages 639–655. Springer, 2012. 2
- [42] Svante Wold, Kim Esbensen, and Paul Geladi. Principal component analysis. *Chemometrics and intelligent laboratory systems*, 2(1-3):37–52, 1987. 4
- [43] Hao Wu and Saurabh Prasad. Semi-supervised deep learning using pseudo labels for hyperspectral image classification. *IEEE Transactions on Image Processing*, 27(3):1259–1270, 2017. 2, 3
- [44] Yi Zhou, Xiaodong He, Lei Huang, Li Liu, Fan Zhu, Shanshan Cui, and Ling Shao. Collaborative learning of semi-supervised segmentation and classification for medical images. In *Proceedings of the IEEE Conference on Computer Vision and Pattern Recognition*, pages 2079–2088, 2019. 3
- [45] Yuliang Zou, Zizhao Zhang, Han Zhang, Chun-Liang Li, Xiao Bian, Jia-Bin Huang, and Tomas Pfister. Pseudoseg: Designing pseudo labels for semantic segmentation. *arXiv preprint arXiv:2010.09713*, 2020. 2, 3, 6, 9